Combustion Science and Technology

ISSN: 0010-2202 (Print) 1563-521X (Online) Journal homepage: www.tandfonline.com/journals/gcst20

Numerical Study on the Radiation Characteristics of Hydrogen-Blended Natural Gas Combustion

Shiquan Shan, Guopei Jin, Xinyi Han, Qi Qin, Leyi Miao & Zhijun Zhou

To cite this article: Shiquan Shan, Guopei Jin, Xinyi Han, Qi Qin, Leyi Miao & Zhijun Zhou (21 Jul 2025): Numerical Study on the Radiation Characteristics of Hydrogen-Blended Natural Gas Combustion, Combustion Science and Technology, DOI: 10.1080/00102202.2025.2536217

To link to this article: https://doi.org/10.1080/00102202.2025.2536217

COMBUSTION SCIENCE AND TECHNOLOGY
https://doi.org/10.1080/00102202.2025.2536217

Taylor & Francis
Taylor & Francis Group

Numerical Study on the Radiation Characteristics of Hydrogen-Blended Natural Gas Combustion

Shiquan Shan, Guopei Jin, Xinyi Han, Qi Qin, Leyi Miao, and Zhijun Zhou

State Key Laboratory of Clean Energy Utilization, Zhejiang University, Hangzhou, China

ABSTRACT

Thermal radiation is one of the main heat transfer mechanisms in boilers. This work numerically investigates the impact of hydrogen-blended natural gas combustion on the radiative heat transfer characteristics of the flame flue gas, to reveal the influence of hydrogen on natural gas combustion and heat transfer. To address the lack of study on radiative heat transfer and applications of accurate radiation models in simulating hydrogen-blended natural gas combustion, this work is conducted based on the newly developed weighted sum of gray gases model (WSGG) for hydrogen-blended natural gas combustion. The multi-physics coupling effect of fuel hydrogen content on radiative heat transfer, temperature distribution, and chemical kinetics are discussed. By constructing a numerical simulation framework, the numerical simulation method was first validated through a thermal companion burner, and then applies it to a numerical study of a 40 kW-class furnace, the influence of 0 ~ 75% hydrogen blending on the radiative heat transfer was systematically analyzed. The results indicate that as the hydrogen blending ratio increases from 0% to 75%, the peak flame temperature rises from 2180.5 K to 2291.8 K, the outlet flame temperature decreases from 864 K to 815 K, and the overall gas effective average absorption coefficient increases, resulting in a radiation ratio increase from 27.22% to 29.42%. The summarization of these qualitative rules and quantitative results has important reference value for the application of hydrogen energy and the optimization of boiler efficiency.

ARTICLE HISTORY
Received 15 March 2025
Revised 2 July 2025
Accepted 15 July 2025

KEYWORDS
Hydrogen-blended natural gas combustion; numerical research; radiative heat transfer; CFD; WSGG model

Introduction

With the transformation of the global energy structure and the enhancement of environmental protection awareness, the development and utilization of clean energy has become a prominent research area. As a relatively clean and efficient fossil fuel, natural gas produces fewer pollutants during combustion. Hydrogen, as a common zero-carbon energy source, is considered an important component of the future energy industry. In order to further promote carbon emission reduction and contribute to the goal of carbon neutrality (Hou et al. 2023), research and application of hydrogen-blended natural gas, an effective way to curb carbon emissions, are of great significance.

Regarding the technology of hydrogen-blended natural gas combustion, researchers have conducted in-depth and detailed studies on combustion characteristics, flame structure and

CONTACT Shiquan Shan shiquan1204@zju.edu.cn State Key Laboratory of Clean Energy Utilization, Zhejiang University, Hangzhou, China
Supplemental data for this article can be accessed online at https://doi.org/10.1080/00102202.2025.2536217

stability, and pollutant emissions. Zhao et al. (2008) found through experiments that hydrogen can significantly decrease the ignition temperature of methane. Choudhuri and Gollahalli (2004) combined numerical simulation and experimental verification, and found that the peak temperature of combustion increases after adding hydrogen in natural gas. El-Ghafour, El-Dein, and Aref (2010) investigated the combustion characteristics of hydrogen-enriched natural gas (with a hydrogen volume ratio of 0–50%) in a free jet turbulent diffusion flame, and the results indicated that hydrogen addition sustains a progressive improvement in flame stability and reduction in flame length. Yoon et al. (2017) studied the effect of fuel composition (a mixture of hydrogen and methane) on combustion instability (CI) frequency and mode shifting (FMS) in a partially premixed model combustor (PP-MC) . In terms of pollutant generation properties, Breer et al. (2023) researched the effect of various hydrogen-methane fuel blending ratios on NO_X production under different combustion conditions and found that the addition of hydrogen only slightly increased the rate of post-flame NO production. Patel and Shah (2019) experimental results showed that the increase of hydrogen concentration in a methane-hydrogen combustion process reduces CO emissions and increases NO_x emissions with a shorter flame length at a constant energy input. Jiang et al. (2018) numerically investigated the formation and destruction of NOx under oxy-fuel combustion of CH_4/H_2 and found the hydrogen addition strengthens the generation pathway of NNH to NO. There are also studies in the specific application scenarios of hydrogen-blended natural gas. Rajpara, Shah, and Banerjee (2018) tested the combustion performance and emissions of methane fuel with the addition of hydrogen based on a laboratory-scale methane-fueled gas turbine combustor. The teams of Zareei, Rohani, and Mahmood (2018) and Fan et al. (2018) explored the application of hydrogen-blended natural gas as fuel for internal combustion engines. Chen et al. (2024) examined the combustion process of hydrogen-blended natural gas in a household gas stove through experiments, including its flame patterns, thermal efficiency, and pollutant emissions. However, current understanding of heat transfer mechanisms in hydrogen-blended natural gas combustion remains insufficient, particularly regarding high hydrogen blending ratios in combustion boiler systems, which requires further comprehensive investigation.

In the combustion process of gas fuels, thermal radiation is one of the main heat transfer models, which has an important impact on the design and optimization of burners. Therefore, scholars have researched the thermal radiation characteristics of hydrogen-blended natural gas. Yang et al. (2018) investigated the effect of turbulence radiation interactions (TRI) on flame temperature, production distribution, and radiative heat transfer in the combustion process of methane/hydrogen blended fuels, and the results showed that the effect of TRI increases the net radiative heat loss and decreases in the flame temperature under high pressure. Zheng et al. (2022) adopted different radiation models to study the effects of radiation reabsorption on the laminar burning velocity of methane/air and methane/hydrogen/air flames, and the results showed that radiation reabsorption promotes the laminar burning velocity, and the addition of hydrogen reduces the impact of radiation reabsorption on the burning velocity. Zenou and Vicquelin (2025) investigated how thermal radiation affects the flame structure and burning velocity through emission and reabsorption for CH_4 and H_2 hybrid combustion flames. Xu et al. (2024) studied moderate or intense low-oxygen dilution (MILD) combustion of hydrogen-enriched methane in a laboratory furnace, examining how radiative and convective heat transfer between gas and wall is affected by the wall temperature as the hydrogen blending ratio

increases from 0% to 100%. Ballester et al. (2009) tested natural gas and hydrogen premixed combustion flames based on a laboratory swirl burner, and experimental results indicated that the intensity of flame's luminous radiation decreases as the hydrogen blending ratio increases. It can be noticed that most of the aforementioned studies are based on laboratory-scale combustion of hydrogen-blended natural gas and are aimed at investigating the effect of thermal radiation characteristics on the combustion process of hydrogen-blended natural gas. However, current research has not systematically investigated the mechanism influence of fuel composition on radiative heat transfer in hydrogen-blended natural gas combustion. Specially, under the application of accurate gas radiation modeling, the coupling effects among radiative heat transfer, temperature distribution, and chemical reaction dynamics under varying hydrogen blending ratios remain inadequately addressed. Furthermore, the characteristics of radiative heat transfer between flue gas and the global furnace wall are rarely reported.

With the rapid development of numerical simulation in recent years, it has gradually become an indispensable tool for the research of combustion. Zohera, Mounir, and Salah (2017) conducted a numerical simulation study of non-premixed turbulent flame of methane-hydrogen using Ansys CFX as a simulation tool, and simulated the combustion phenomena separately adopting Eddy Dissipation model (EDM), and Finite Rate Combustion (FRC) model combined with EDM, but the radiation model settings were not specified. Wang et al. (2024) used ANSYS Fluent to conduct numerical simulations to investigate the combustion characteristics and emission generation of premixed NH_3/air and CH_4/air jet flame, and the eddy dissipation concept (EDC) model was chosen to solve the slow reactions in the MILD combustion, at the same time the effectiveness of the computational fluid dynamics (CFD) results was verified by experimental data. Gheshlaghi and Tahsini (2023) numerically simulated the methane-hydrogen premixed combustion with the standard $k-\varepsilon$ model chosen for the turbulence model and GRI-Mech 2.11 for the combustion mechanism, but the shortcoming was that the effect of radiation source term was neglected and no radiation model was adopted in this simulation. Büyükakın and Öztuna (2020) used Fluent code to simulate the methane-hydrogen hybrid combustion process in a household back-pressure boiler, with the discrete coordinate method for radiation modeling, and the results were verified by flue gas temperature and emission concentration obtained from experiments. Wang et al. (2014) calculated the radiative heat transfer of a hydrogen/methane jet flame by using the finite volume method and verified the reliability of the open-source CFD code FireFOAM by comparing it with several experimental results in the literature. Several studies related to thermal radiation mentioned above (Yang et al. 2018; Zenou and Vicquelin 2025; Zheng et al. 2022) also adopted numerical simulation or a combination of experimental and numerical simulation methods. At present, numerical simulation research aimed specifically at the thermal radiation characteristics in the field of hydrogen-blended natural gas combustion still needs to be developed. The gas radiation models used in the research are mainly based on the gray body assumption or conventional air combustion condition models. Particularly under complex conditions such as high hydrogen blending ratios, the accuracy of thermal radiation numerical simulations is difficult to ensure. In recent years, Jin et al. (2024) have developed a new WSGG model suitable for high hydrogen blending ratios in natural gas combustion, however no research has yet been conducted on the combustion radiation characteristics using these models.

To address the above research gaps, this paper numerically investigates the thermal radiation release characteristics of hydrogen-blended natural gas combustion based on CFD numerical simulation. The newly developed WSGG model of hydrogen-blended natural gas combustion is constructed and UDF code is written into the CFD program to perform simulation and its results are compared with the experimental results. Furthermore, for a 40 kW hot co-flow combustor, the radiative heat transfer characteristics of hydrogen-blended natural gas during combustion are investigated through numerical simulation using the newly developed WSGG model and detailed chemical reaction kinetics. The combustion field temperature variations, product concentration distributions and radiation characteristics are quantitatively explored for different hydrogen blending ratios in this combustor, and then net radiative heat loss and radiative fraction are calculated. This study elucidates the multi-physics coupling mechanisms underlying fuel composition variations in radiative heat transfer, temperature distribution, and chemical kinetics within combustion chambers. By investigating the characteristics of radiative heat transfer between flue gases and global furnace walls, it establishes fundamental principles for optimizing hydrogen-blended combustion systems in natural gas boiler applications.

Models and methods

Governing equations

The governing equations of the flow field are the reaction conservation equations in the XY rectangular coordinate system. To simplify the mathematical treatment of the issue, the following assumptions are made:

- The reaction flow is steady.
- The effect of gravity (buoyancy) is neglected.
- Heat generated from viscous shear is neglected (Br << 1).

In the simulation of hydrogen-blended natural gas combustion, it is necessary to follow the basic governing equations including the mass conservation equation (continuity equation), momentum conservation equation, energy conservation equation, and component conservation equation (Poinsot and Veynante 2005). The simplified governing equations are given in their differential form as follows.

Mass conservation

In a selected infinitesimal element, the reduction in mass due to changes in fluid density over a unit time is equal to the total mass of the fluid that flows out of that element body during the same time interval, which is the principle of mass conservation:

$$\frac{\partial \rho}{\partial t} + \nabla \cdot (\rho u) = 0 \tag{1}$$

Under the steady state conditions set in this work, the mass conservation equation is expressed as:

$$\nabla \cdot (\rho u) = 0 \tag{2}$$

where $u = u_x + u_y$, and the three terms are velocity and velocity components in the X and Y directions, m/s, ρ is density of the fluid, kg/m^3.

Momentum conservation

According to Newton's second law, the rate of momentum change of the fluid in a element body is equal to the sum of the external forces acting on that element body. Under steady state conditions, the momentum conservation equations in the X and Y directions are expressed as:

$$Xdirection : \nabla \cdot (\rho u_x \vec{u}) = -\frac{\partial p}{\partial x} + \frac{\partial \tau_{xx}}{\partial x} + \frac{\partial \tau_{yx}}{\partial y} + \rho f_x \tag{3}$$

$$Ydirection : \nabla \cdot \left(\rho u_y \vec{u}\right) = -\frac{\partial p}{\partial y} + \frac{\partial \tau_{xy}}{\partial x} + \frac{\partial \tau_{yy}}{\partial y} + \rho f_y \tag{4}$$

where p is pressure on the element body, Pa, τ is viscous force on the surface of the element body, Pa, f is body force per unit mass in each direction, m/s^2.

Energy conservation

According to Newton's second law, the rate of momentum change of the fluid in a element body is equal to the sum of the external forces acting on that element body. Under steady state conditions, the momentum conservation equations in the X and Y directions are expressed as:

On this foundation, the energy conservation equations under steady state conditions are derived (Kuo 1986; Poinsot and Veynante 2005), which is, the energy increase of the fluid element is equal to the sum of the net heat flow into the element and the work done on the element by body forces and surface forces:

$$\nabla \cdot (\vec{u}(\rho E + p)) = \nabla \cdot \left(k_e \nabla T - \sum_{k=1}^{N} h_k J_k + (k_e \vec{u}) \right) + S_k \tag{5}$$

$$\begin{cases} E = h - \frac{p}{\rho} + \frac{u^2}{2} \\ h_k = \int_{T_0}^{T} C dT \end{cases} \tag{6}$$

where k_e is heat transfer coefficient of the fluid, W/(m·K), T is temperature, K, E is the sum of internal energy, potential energy and kinetic energy of the fluid element, J/kg, h is enthalpy, J/kg, S_k is volume heat source term.

Component conservation equation

Component conservation means that in a element, the rate of mass change of a certain chemical component i is equal to the rate of component i entering into the element and the rate of chemical reaction to produce component i, and the equation is expressed as:

$$\frac{\partial}{\partial t}(\rho Y_i) + \nabla(\rho \vec{u} Y_i) = -\nabla \cdot \vec{J}_i + R_i + S_i \tag{7}$$

where Y_i is volume fraction of component i, $\vec{J}_i$ is diffusive flux, R_i is the net production rate of component i in chemical reaction, S_i is source term.

Reaction mechanism

The combustion reaction kinetic minima grid mechanism CKL1.1 (Ren, Wang, and Li 2021) is adopted as the reaction mechanism in this study, which considers in detail a variety of intermediate products and reaction paths in the methane combustion process, containing 18 components with a total of 22 steps of reaction, and is able to simulate the chemical reaction process of hydrogen blended natural gas jet combustion accurately. The reaction mechanism is based on the principle of chemical equilibrium, featuring dual parameters, full reversibility, wide temperature conditions and NOx generation. Meanwhile, the chemical resolution of the mechanism is controlled based on the miniaturization network method, and the number of elementary reactions is compressed under the premise of keeping the number of chemical species unchanged, which is of great significance for the practical engineering calculations. Detailed combustion mechanism can be found in Appendix Table A1.

Radiation Model

The weighted sum of gray gases (WSGG) model is a simplified method for simulating the radiative properties of non-gray gases. The core idea is to approximate the radiative behavior of actual non-gray gases by introducing hypothetical gray gases (gas with a constant spectral absorption coefficient), simplifying the calculation process. Compared with more advanced Full-Spectrum k-distribution (FSK) or the Spectral Line Weighted-sum-of-gray-gases (SLW) models which are also employed for combustion scenarios involving participating media like H_2O and CO_2, the WSGG model continues to be widely employed in commercial CFD software due to its sufficient accuracy in capturing key physical phenomena, higher computational efficiency, and more compact formulation (da Fonseca et al. 2023). In the WSGG model, each gray gas represents a specific spectral band, and its weight reflects the relative importance of that spectral band in the overall radiation process. At path-length L and pressure P, the emissivity of non-gray gas is represented by the weighted sum of the emissivity of several gray gases (Hottel and Sarofim 1967):

$$\varepsilon = \sum_{i=1}^{n} a_i \left[1 - exp\left(-k_{p,i} XPL\right)\right] \tag{8}$$

where a_i is weight, the weight of transparent gas a_0 corresponds to the absorption coefficient $k_0 = 0$, and the sum of all weights must be 1, $\sum_{i=1}^{n} a_i = 1$. X is the sum of mole fractions of H_2O and CO_2 in the gas mixture, and it is expressed as $X = X_{H_2O} + X_{CO_2}$. CH_4 is not considered because of its weak radiative capacity in atmospheric conditions (Ju, Masuya, and Ronny 1998). Meanwhile, the unburnt CH_4 only exists in a small region near the nozzle, which can be reasonably ignored in the global radiation heat transfer calculation. The key of

WSGG model is to determine the absorption coefficient $k_{p,i}$ and the weight coefficient a_i. In the traditional WSGG model, the weight value a_i is mainly related to the temperature and is expressed as a temperature polynomial of degree m:

$$a_i = \sum_{j=0}^{m} c_{i,j} \left(\frac{T}{T_{ref}} \right)^j \tag{9}$$

where T_{ref} is reference temperature. This study adopts the WSGG model provided by the literature (Jin et al. 2024), which is mainly developed for hydrogen blended natural gas combustion environment, and the model structure is modified according to the application requirements of the actual pressure varying conditions. Containing four gray gases and a transparent window, the improved new WSGG model can be adaptable to the calculation of the radiative properties of natural gas combustion at up to 75% hydrogen blending ratio and can be used for a range of total pressures from 1 to 10 bar. According to Jin et al. (2024), the weight coefficients are expressed as the sum of the multiplication of polynomial functions of temperature T and pressure P:

$$w_i(T, P) = a_i(T) b_i(P) \tag{10}$$

By reference to the definition of weight coefficients in the original model, in this paper, the temperature polynomial function $a_i(T)$ and the pressure polynomial function $b_i(P)$ are respectively expressed as J_1 polynomials of temperature T and J_2 polynomials of total pressure P:

$$a_i(T) = \sum_{j=0}^{J_1} \alpha_{i,j} \left(\frac{T}{T_0} \right)^j \tag{11}$$

$$b_i(P) = \sum_{j=0}^{J_2} \beta_{i,j} \left(\frac{P}{P_0} \right)^j \tag{12}$$

where $\alpha_{i,j}$ and $\beta_{i,j}$ are temperature polynomial coefficient and pressure polynomial coefficient of the emission gas, respectively, T_0 is the reference temperature with a value of 2000 K, and P_0 is the reference pressure with a value of 1 bar.

In the work by Jin et al. (2024), the performance of the modified WSGG model and the default WSGG-Smith model in Fluent (Smith, Shen, and Friedman 1982) was discussed in terms of emissivity and one-dimensional radiative heat transfer calculations. The results demonstrated that the modified WSGG model provides higher accuracy when predicting the radiative properties of hydrogen-enriched natural gas combustion products. As shown in Figure 1, for gas emissivity calculations at 10 bar, 1500 K, and with 75% hydrogen-blended natural gas, the average error of the modified model compared with the benchmark statistical narrow band (SNB) model is only 1.75%, whereas the WSGG-Smith model exhibits significant deviations, exceeding 30% at higher partial pressure path lengths.

The newly developed WSGG model is used in Fluent by packaging into a user-defined function (UDF). In practical applications, according to previous work experience (Shan et al. 2018; Yin et al. 2010), the calculation of different H_2O/CO_2 molar ratio gas environments can be applied through a specific table, as shown in Table 1. This method has the advantages of being formally simple and convenient, and although there are certain errors,

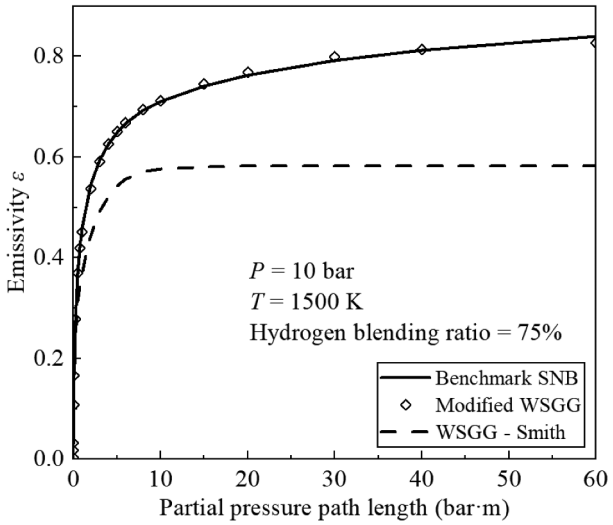

Figure 1. Emissivity calculated using the modified WSGG model and WSGG-Smith model.

Table 1. The compilation method of new-WSGG model in UDF.

Condition	Strategy	Prameter Selection
If($M \leq 2.67$)	Use parameters for	$M = 2.25$
If($M \leq 3.38$)	Use parameters for	$M = 3$
If($M \leq 4.22$)	Use parameters for	$M = 4$
else	Use parameters for	$M = 5$

it is not obvious. Therefore, it is one of the methods to be preferred Yin et al. (2010); Shan et al. (2018). The Discrete Ordinates (DO) model is employed for radiative heat transfer. In this steady-state RANS simulation, where time averaging is used, the turbulence–radiation interaction (TRI) is neglected.

Numerical modeling of combustion furnace

Hot co-flow combustor modeling

In order to verify the rationality of the numerical method coupling new WSGG radiation model and combustion mechanism in CFD simulation calculations in this study, the combustion field simulation is conducted by applying the hot co-flow combustor (Dally, Karpetis, and Barlow 2002) and compared with the experimental data. In the combustion experiment setting described in the reference, the cylindrical burner is placed in a wind tunnel. The fuel pipe of the hot co-flow burner has an inner diameter of 4.25 mm, and upstream of outlet plane of the fuel pipe, a secondary burner is designed with an inner diameter of 82 mm. In order to minimize the heat loss of combustion process to the surrounding environment, the outer ring of burner is made of ceramic belt as a heat insulation material. The entire burner is placed in the wind tunnel to provide room temperature air at the same speed as the hot co-flow. This design ensures that the combustion process is carried out in a stable airflow environment, which helps reduce the impact of

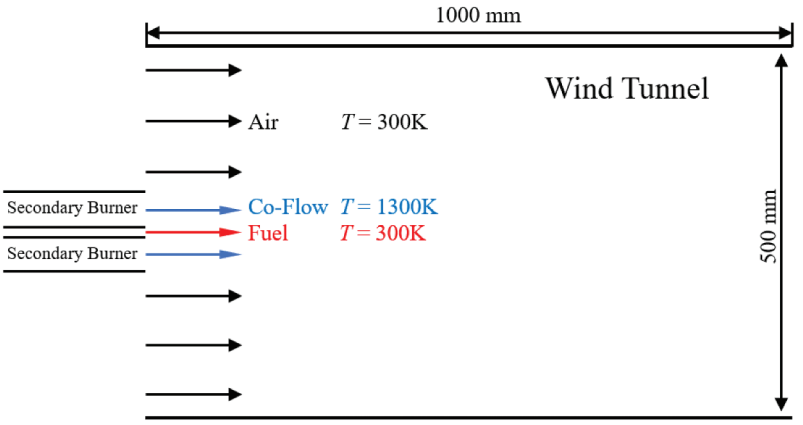

Figure 2. Hot co-flow combustor burning area flowing field modelling diagram.

external disturbances on the experimental results. In order to further study, the combustion characteristics and radiation heat transfer of this combustion device, a 500 mm × 1000 mm combustion area is delineated at the exit of the combustion flame, as shown in Figure 2. The detailed grid distribution is shown in Figure S1 in the Appendix.

In the modeling process, SpaceClaim software is used, and quadrilateral structured grid is selected in the grid division stage. In order to ensure the accuracy of simulation and simplify the calculation amount, the density distribution of grid is specially set in this study. Starting from the entrance and axis, the grid density gradually turns from dense to sparse outward. In the test conditions, CH_4 is used as fuel with a flow rate of 70 m/s, and air is used for oxidant with a flow rate of 2.5994 m/s. Multiple calculations are carried out under different grids to compare the maximum combustion temperatures, as shown in Figure 4(a), it is found that the maximum temperatures tend to be constant when the number of grids exceeds 142,437, indicating that further increase in the grid density do not significantly affect the accuracy of simulation results anymore. Therefore, the model with a grid number of 142,437 is chosen in subsequent studies to reduce the computational complexity while maintaining the simulation accuracy.

40 kW hydrogen-blended natural gas combustion furnace numerical modeling

Based on a hot co-flow combustor (Dally, Karpetis, and Barlow 2002), the variation of radiative heat transfer with hydrogen blending ratio of natural gas is investigated. In order to study the heat transfer problem in the combustion chamber, the furnace structure is established. The inner diameter of fuel pipe is 4.6 mm, the inner diameter of co-axial oxidant pipe is 82 mm, and the total length of fuel nozzle is 50 mm, of which the part close to combustion furnace is designed to have an expansion area with a length of 20 mm and a flaring angle of 40°, and this design helps to optimize combustion by sufficiently mixing fuel with oxidant. The furnace itself adopts an axial symmetrical structure with a length of 1250 mm and a diameter of 400 mm. The volume heat load is about 300 kW/m^3, which meets the gas boiler requirement standard. The outlet of the furnace chamber is designed as a cylinder structure with a length of 100 mm and an exhaust port diameter of

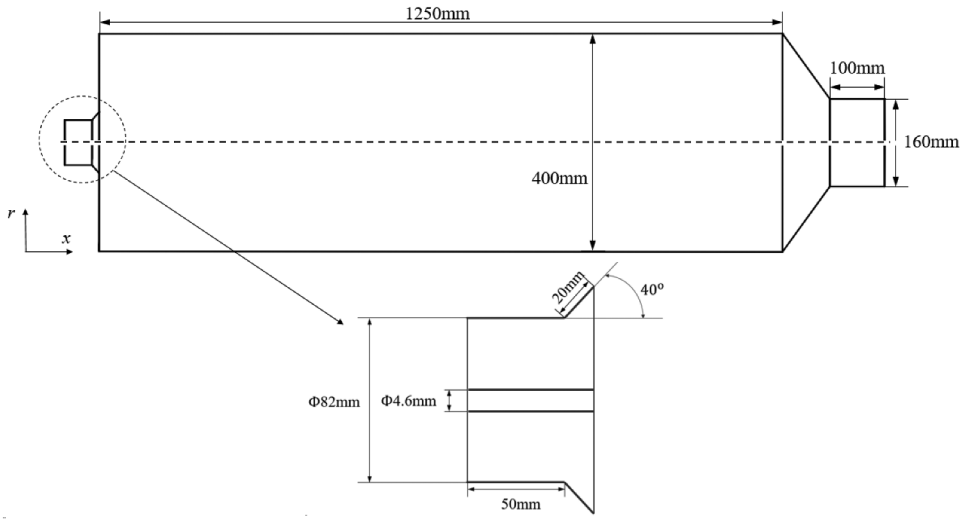

Figure 3. 40 kW combustion furnace simplified model section schematic.

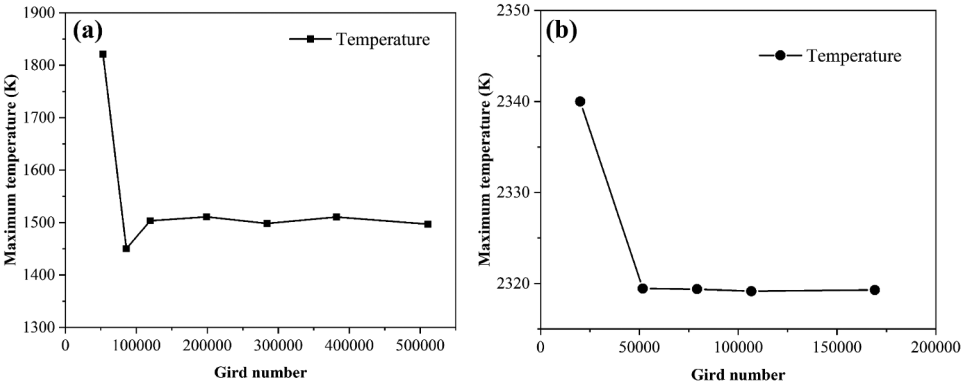

Figure 4. Grid independence verification: (a) hot co-flow combustor; (b) 40 kW combustion furnace.

160 mm. The section schematic of simplified furnace model is shown in Figure 3, and the detailed grid distribution is provided in Figure S2 in the Appendix.

In this study, SpaceClaim software is adopted for grid division and quadrilateral structured grid is selected. In order to simplify the calculation while ensuring accuracy, the grids near fuel inlet and axis are processed to increase the density. The test conditions are simulated by using the methane single-step combustion reaction model in Fluent software with the same boundary conditions. The flow rate of fuel input (CH_4) is 60 m/s, and the flow rate of oxidant (air) is 2.23 m/s. As shown in Figure 4(b), by comparing the maximum combustion temperatures simulated by different grid models, it is found that when the number of grids exceeds 52,239, the increase in grid density no longer has a significant impact on accuracy of the results. Therefore, a model with grids of 52,239 is selected for subsequent simulation.

Table 2. Designed working cases.

Fuel			Oxidant			
Atmosphere			Atmosphere			
V CH_4	V H_2	Flow rate (m/s)	V O_2	V N_2	Flow rate (m/s)	Excess air ratio
100%	0%	78.62	21%	79%	2.9195	1.1
90%	10%	78.62	21%	79%	2.7005	1.1
80%	20%	78.62	21%	79%	2.4816	1.1
70%	30%	78.62	21%	79%	2.2626	1.1
60%	40%	78.62	21%	79%	2.0436	1.1
50%	50%	78.62	21%	79%	1.8247	1.1
30%	70%	78.62	21%	79%	1.3868	1.1
25%	75%	78.62	21%	79%	1.2773	1.1

Set the numerical solution method

In simulating the combustion process, this study employs a variety of numerical models and solution methods aimed at accurately calculating complex phenomena such as turbulence, radiative heat transfer, and chemical reactions. The standard *k*-epsilon model is applied based on the properties of turbulent field. For the chemical reaction kinetics in the combustion process, the Eddy Dissipation Concept (EDC) model is selected, which is based on the interaction between turbulent eddy groups and chemical reactions, and is able to fully take into account the effect of turbulence on the chemical reaction rate, more realistically reflecting the mechanism of chemical reactions in the combustion process. For the solution strategy, a pressure-based separation solver is chosen and the discretized equations are solved in linearized implicit format. The momentum, turbulent kinetic energy, and turbulent dissipation rate equations are discretized using the first-order upwind format, while the second-order upwind format is chosen for the other governing equations. The combustion reaction mechanism is chosen to be CKL1.1. In addition, the linearized discrete equations are solved in implicit format. The COUPLE algorithm is used for iterative solution. For the simulation of radiative heat transfer, the WSGG model (Jin et al. 2024) of hydrogen blended natural gas combustion is employed, which can more accurately consider the changes in radiative characteristics of gas medium caused by the changes in component field, and can be more adapted to the combustion of natural gas with a high proportion of hydrogen blended, thus improving the simulation accuracy of the radiative heat transfer process in the combustion furnace.

The convergence criterion of this work is achieved when the order of magnitude of the residuals of governing equations reaches 10^{-3} for continuity, 10^{-6} for DO-intensity and energy. Moreover, fluctuations of area-weighted average of mole fraction of CO_2 at the furnace outlet to be less than 10^{-3} is monitored as additional criteria.

Investigating cases design

In this study, H_2/CH_4 volumetric blending ratios of $0 \sim 75\%$ are selected for the combustion reaction with air, and eight groups of working cases are set. The hydrogen blending ratio is denoted by *HBR*. Fuel is set as velocity flow rate inlet

at 300 K, oxidant injection temperature is 800 K, and the wall temperature is set to 800 K by calculation. The designed working conditions for each group are shown in Table 2.

Results and discussion

Experimental verification for numerical simulation method of hydrogen blended natural gas combustor

In order to check the rationality of the numerical simulation method used, verification calculation is carried out in this study using the same burner conditions in reference (Dally, Karpetis, and Barlow 2002). In the comparison experiments, the same fuel and oxidant conditions are set, in which the fuel consists of 88.9% CH_4 and 11.1% H_2 at 300 K, while the oxidant consists of 79% N_2, 9% O_2, 6.5% H_2O and 5.5% CO_2 at 1300 K, where the gas compositions of each part are the mass fractions. In this paper, the radial temperature distributions and the concentration distributions of different substances is compared for both at $x = 30$ mm.

The radial distributions of average temperature and mass fractions of OH, O_2 and H_2O at the axial position $x = 30$ mm are given in Figure 5. Numerical simulation results of radial temperature at axial position $x = 30$ mm are given in Figure 5(a) and compared with

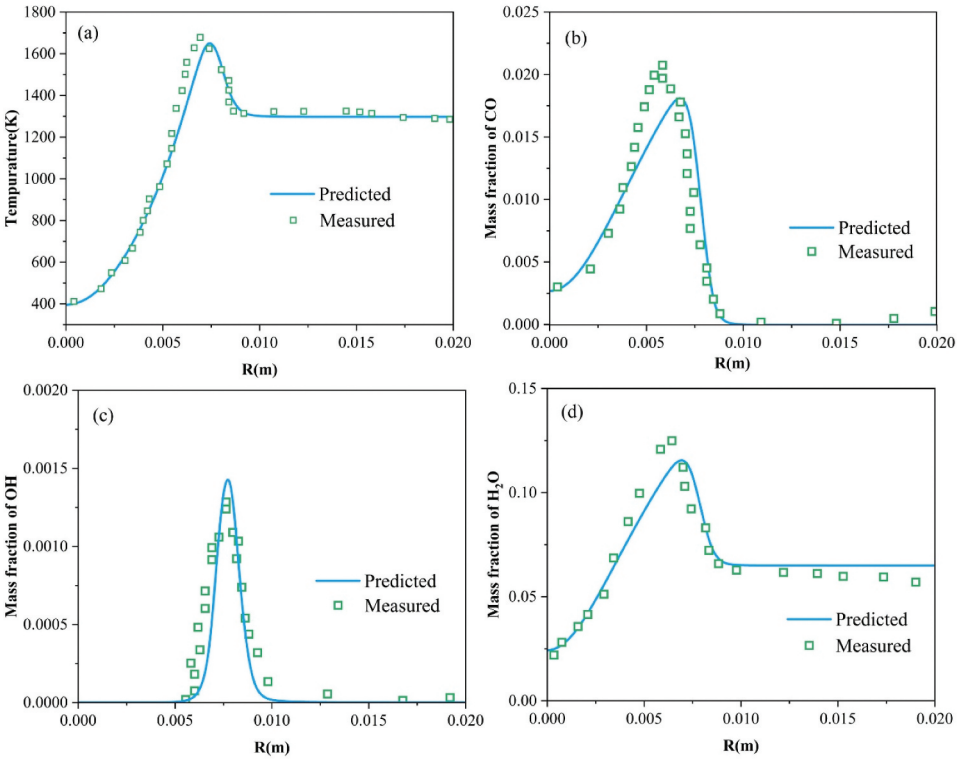

Figure 5. Numerical simulation results compared with experimental results of natural gas hydrogen blended combustor.

published experimental measurements in reference (Dally, Karpetis, and Barlow 2002). The results show that the radial temperature is consistent with the measurement results in trend. Figure 5(c,d) show the general consistency of the predicted OH and H_2O results with the actual measured values. However, Figure 5(b) shows that numerical simulation underestimates CO produced by experimental combustion, with some discrepancies observed between two mass fraction peaks. On the experimental side, cooling and extinction effects of secondary premixed flame in the co-flow could lead to CO uncertainties (Christo, Szego, and Dally 2005). On the numerical side, potential sources of error include the turbulence model hypothesis and chemical mechanism simplification. Overall, the numerical simulation method coupled with the new WSGG radiation model can provide good prediction results in predicting temperature gradient and gas mass ratio distribution. Therefore, the rationality of the numerical simulation method based on the new WSGG radiation model for calculation of hydrogen blended natural gas combustion conditions can be ensured and can be applied to subsequent simulation of the hot co-flow combustor.

Numerical simulation results of 40 kW combustion furnace radiation characteristics

The numerical simulations of 40 kW combustion furnace with different hydrogen blending ratios are compared, with all cases calculated at a fuel flow rate of 78.62 m/s. For pure methane combustion, the fuel flow rate is 0.86 g/s, the theoretical combustor power is 44.70 kW, and the actual effective thermal power of combustor is about 40 kW. Since the density of hydrogen is much less than that of methane, the mass fraction of methane is higher than 0.72 even when the volume fraction of hydrogen in the fuel mixture reaches 75%. In addition, hydrogen has a lower unit molar calorific value per unit volume compared with methane. Thus, mixed fuels with different hydrogen blending ratios may have different fuel flow rates and total heat inputs. As shown in Figure 6, when hydrogen is blended with methane, the fuel mass flow rate and heat input decreases continuously as the hydrogen percentage increases. The calculation results give the effect of hydrogen percentage on the combustion of hydrogen/methane blended fuels at a constant fuel injection rate.

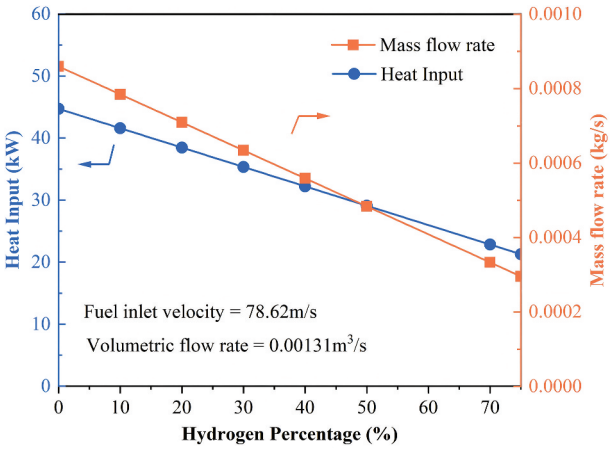

Figure 6. Variation of fuel mass input and heat input as the hydrogen blending percentage.

Table 3. Comparison of simulation with and without radiation.

H_2 Blending Ratio	Case	Total Wall Heat Flux (kW/m^2)	Radiation Wall Heat Flux (kW/m^2)	T_max (K)	T_outlet (K)
0%	With Radiation	9.390	7.747	2180.5	864.0
0%	No Radiation	6.392	0	2196.3	1264.7
10%	With Radiation	8.798	7.281	2188.2	856.3
10%	No Radiation	6.106	0	2204.3	1242.9

The importance of radiation effect

Thermal transport within the combustion chamber fundamentally operates through radiation and convection, and therefore the radiative effects cannot be easily neglected. In this section, we compare the simulations with and without radiation to demonstrate the impact of radiation on the flow field. Both without and with hydrogen (10%) are considered to investigate the overall impact of radiation on the wall heat flux. The results are shown in Table 3.

The difference in the average outlet gas temperature between considering and neglecting radiation effects can reach approximately 400 K. According to the Stefan-Boltzmann law, a 400 K difference is sufficient to demonstrate the presence of strong radiative heat transfer effects.

From the perspective of wall heat flux, for the case of 10% hydrogen addition as example, neglecting radiation leads to a 0.7% overestimation of the peak flame temperature, a 46.3% overestimation of the exit gas temperature, and a 31.9% underestimation of the total wall heat flux. This discrepancy occurs because when radiation is not considered, heat transfer relies solely on convection. The inclusion of radiation introduces an additional mode of heat transfer, leading to an increase in the total radiative heat flux. Radiative heat transfer removes some of the energy from the flame and the exhaust gases, thereby suppressing the peak flame temperature. Furthermore, the increase in the total radiative heat flux results

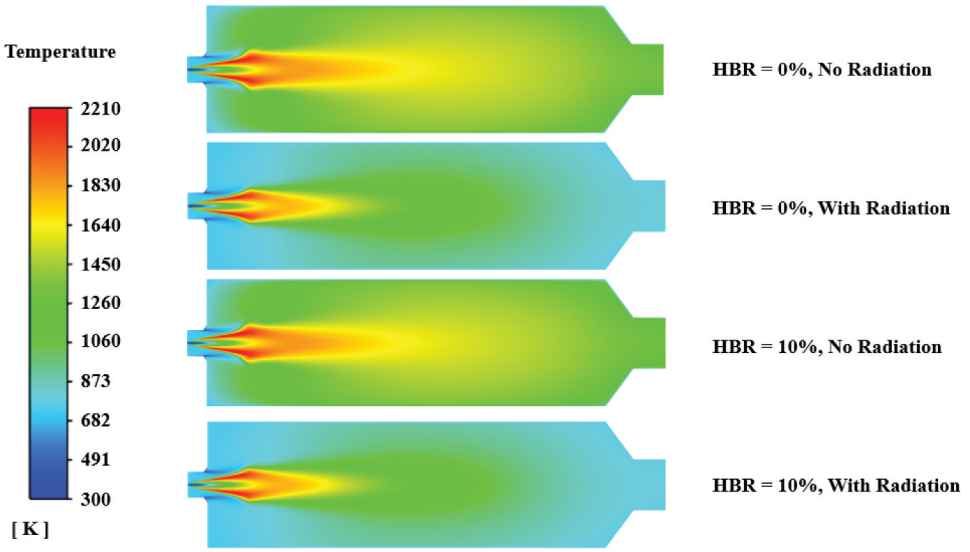

Figure 7. Combustion temperature distribution with and without radiation.

in more heat being lost through the walls, leading to a decrease in the outlet gas temperature. The temperature field distribution under these four conditions is shown in Figure 7.

The comparative simulation results, including and excluding radiation effects, demonstrate that radiative effects play a crucial role in combustion processes, while also indirectly shows the importance of applying accurate radiation characteristic model in simulation calculation.

Combustion temperature field analysis

First, from the perspective of temperature, an important parameter to characterize the combustion reaction, the temperature contour and axial temperature distribution of the combustion reaction under different hydrogen blending ratios cases are shown in Figures 8 and 9(a). The peak combustion temperatures, average outlet temperatures and average

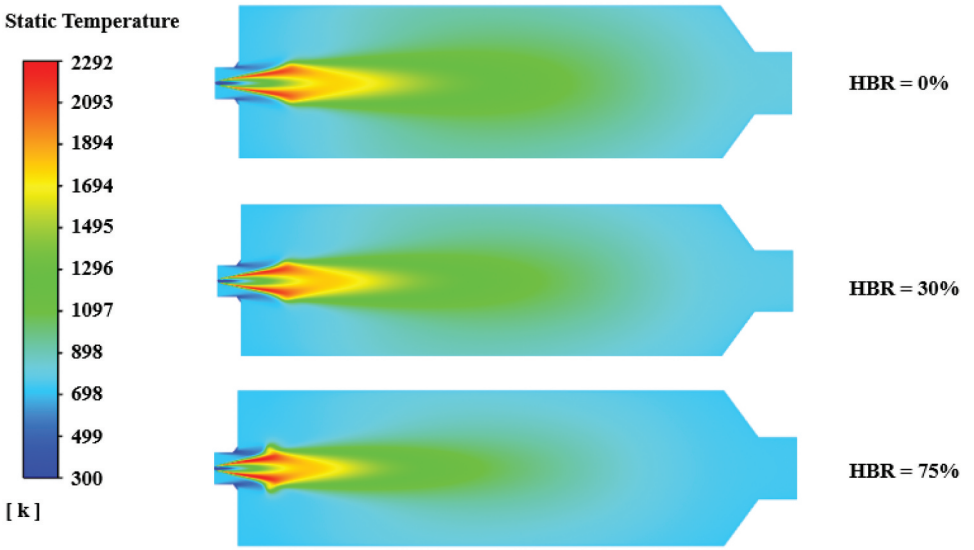

Figure 8. Combustion temperature distribution contour at each hydrogen blending case.

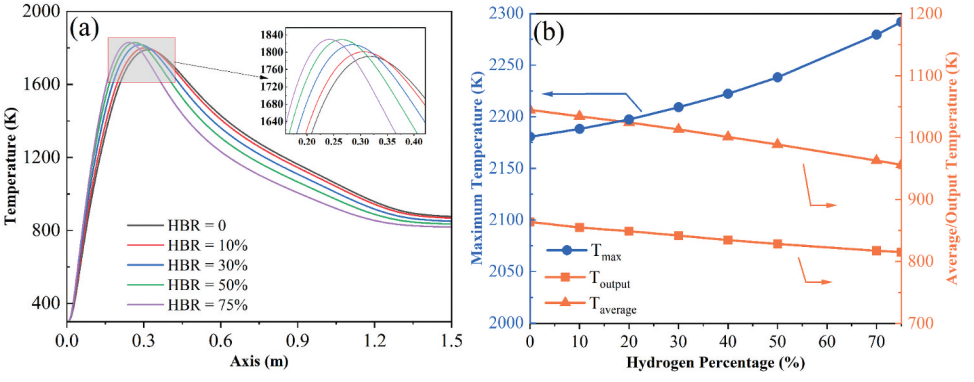

Figure 9. Combustion with different hydrogen blending ratios (a) axial temperature of the combustion furnace; (b) maximum, outlet and average temperature distributions.

combustion zone temperatures of different hydrogen blending ratios are listed at the same time in Figure 9(b). It is evident that with the increase in the hydrogen blending ratio, the peak temperature achieved by flame combustion shows a significant upward trend. At the same time, the temperature of the high-temperature zone also rises with the increase in the hydrogen blending ratio, and this high-temperature zone gradually tends to concentrate near the fuel inlet. Toward the combustion outlet, the temperature exhibits a gradual decline. Considering that hydrogen has a lower activation energy than methane, it demonstrates greater reactivity in chemical reactions, facilitating its reaction with oxygen (O_2). Consequently, as the hydrogen blending ratio increases, the exothermic combustion reaction is initiated earlier, leading to the high-temperature zone progressively moving toward the fuel inlet.

Secondly, from the perspective of combustion reaction mechanisms, the reaction process between hydrogen and oxygen is relatively simple, with fewer intermediate steps, such as the conversion process of $H_2 \rightarrow HO_2/H \rightarrow OH \rightarrow H_2O$. In contrast, the reaction between methane and oxygen involves more intermediate products, making the reaction mechanism more complex. Therefore, the reaction between hydrogen and oxygen is more intense, and the rate of heat release during combustion is faster, which further explains why hydrogen blending leads to an increase in combustion reaction temperature and the phenomenon of the high-temperature region occurring earlier. Thirdly, from the perspective of calorific value, although the low calorific value of methane (35.88 MJ/Nm^3) is higher than that of hydrogen (10.79 MJ/Nm^3), the overall heat load of the mixed fuel shows a decreasing trend as the hydrogen blending ratio increases. This indicates the total heat released during the complete combustion of the mixed fuel is decreasing. Therefore, as the hydrogen blending ratio increases, the corresponding decrease in the outlet temperature aligns with the trend of the average temperature variation within the combustion zone.

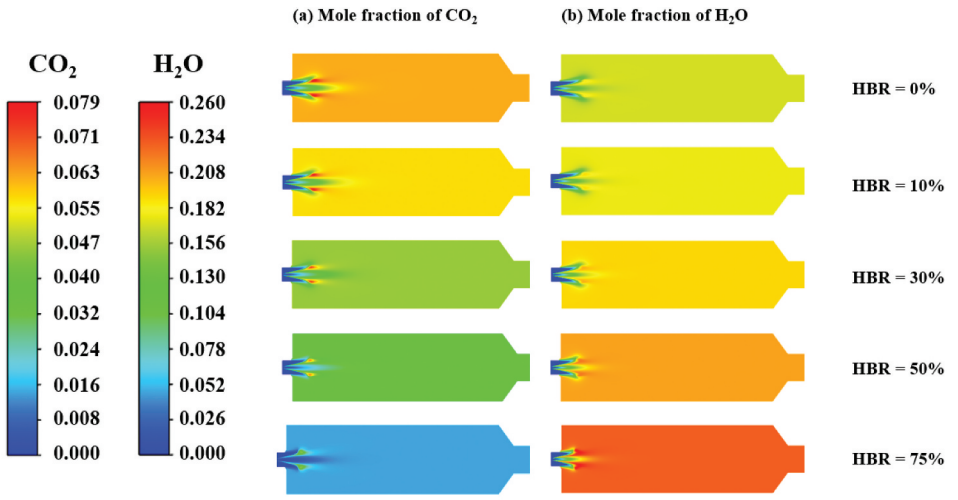

Figure 10. Under the conditions of each hydrogen blending ratio (a) CO_2 concentration distribution contour (b) H_2O concentration distribution contour.

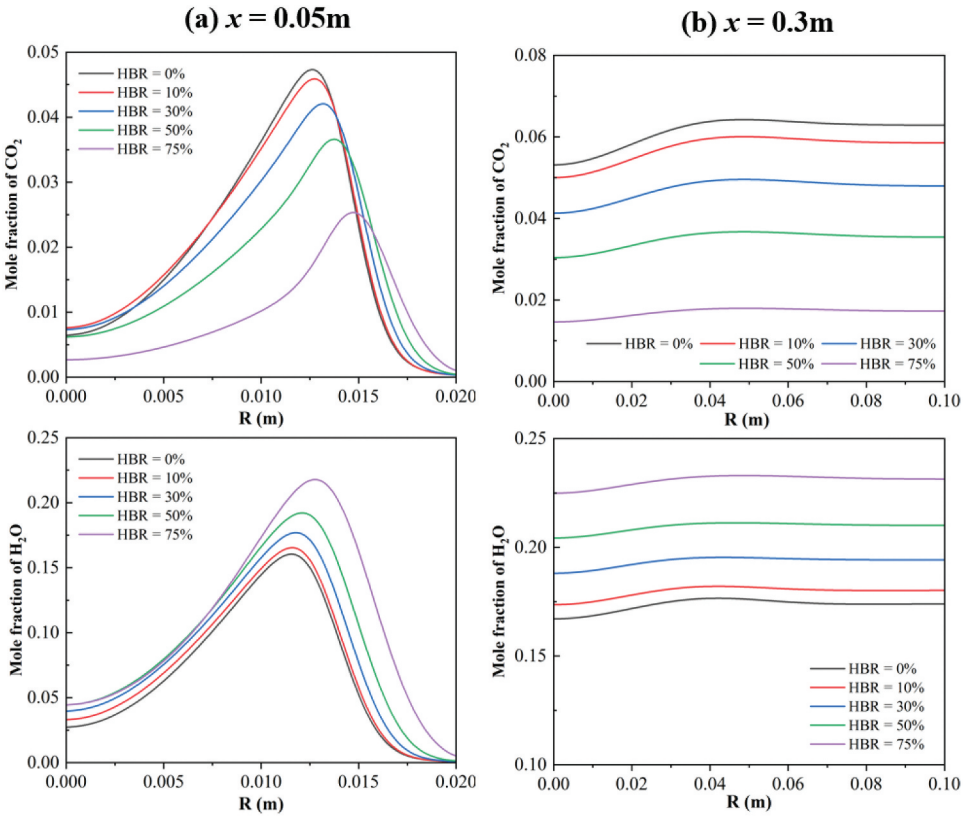

Figure 11. Distribution of CO_2 and H_2O molar fractions along the radial direction for each hydrogen blending ratio case.

Effect of hydrogen blending ratio on combustion products

The primary combustion products of methane-hydrogen mixtures are H_2O and CO_2. Figure 10(a) shows the effect of the hydrogen blending ratio on the concentration of CO_2 in the combustion products. With the increase in the hydrogen blending ratio, the CO_2 concentration progressively declines due to the change in the composition of the original methane fuel caused by the addition of hydrogen. As the proportion of blended hydrogen increases, the methane (CH_4) content in the mixed fuel correspondingly decreases. Since methane is a carbon-containing fuel, the decrease in its content directly results in a reduction in the total carbon (C) content in the fuel. During the combustion process, carbon is primarily converted into CO_2. Therefore, when the carbon content in the mixed fuel decreases, the amount of CO_2 generated in the combustion reaction products also decreases accordingly. Moreover, the contour reveals the regional characteristics of CO_2 concentration changes during combustion, with the variation in CO_2 concentration mainly occurring in the axial distance range of $x = 0 \sim 0.4$ m. This region is the primary area where the combustion reaction occurs, where the fuel and oxidant are fully mixed and combustion takes place. As the combustion reaction proceeds, the main concentration region of CO_2 generation shrinks with the reduction in carbon content. Beyond $x = 0.4$ m, the combustion reaction is essentially complete, and the remaining fuel gas and combustion products

diffuse and mix within the combustion chamber. As a result, in this region, the CO_2 concentration approaches a stable state, with no further significant variations.

As shown in Figure 10(b), the concentration of H_2O gradually increases as the hydrogen blending ratio increasing, with the variation in the mixed fuel composition being the primary contributing factor. With the rising proportion of hydrogen blending, the hydrogen (H) content in the fuel gas increases, and the hydrogen element is mainly converted into H_2O. Therefore, the increase in hydrogen content in the fuel gas directly leads to a higher production of H_2O in the combustion reaction products. The results show that the variation in H_2O concentration primarily takes place within the axial distance range of $x = 0 \sim 0.3$ m. This zone is the main area for the initial combustion reaction, in which hydrogen mixes rapidly with the oxidant and combustion occurs. Due to the fast chain reaction rate of H_2 combustion, the generation of H_2O is also more rapid, resulting in the stabilization of H_2O closer to the inlet. In the region where $x > 0.3$ m, the combustion reaction is essentially complete, and the concentration in the combustion chamber approaches a stable state.

To further investigate the patterns of hydrogen-blended natural gas combustion reactions across different flame regions, two key positions during the combustion process are selected: $x = 0.05$ m (front part) and $x = 0.3$ m (rear part), and the radial distribution of components at these positions are analyzed, as shown in Figure 11. First, with a constant volumetric fuel flow rate, the increase in hydrogen concentration results in a decrease in the mass flow rate and energy input of the fuel mixture, causing a reduction in the axial velocity and rate of the chemical reaction. Therefore, at the front part of the combustion reaction ($x = 0.05$ m), the radial position, where the product gases CO_2 and H_2O reach their peak concentrations, will move backward. Second, the reduction in the carbon production species CO_2 is primarily due to the substitution effect of hydrocarbons, with the chemical kinetic effect playing a relatively smaller role. This means that during hydrogen-blended combustion, the reduction in CO_2 is mainly due to hydrogen replacing part of the methane, rather than a change in the chemical reaction rate. Additionally, the addition of hydrogen leads to a relatively shorter flame length, which becomes especially noticeable at higher hydrogen concentrations due to the high reactivity of hydrogen. With the addition of hydrogen, the reaction zone moves upstream, further influencing the flame's shape and length. Finally, at the rear part of the combustion reaction ($x = 0.3$ m), the fuel and oxidant have been fully mixed and the combustion process is completed, resulting in the stabilization of the product gas concentrations.

Effect of hydrogen blending ratio on radiation characteristics

In this work, the effective average absorption coefficient $\bar{\kappa}$ is used to evaluate the global radiative heat transfer that equivalently characterizes the overall radiative absorption capability under given temperature, composition, and optical path length conditions. Specifically, based on the Lambert-Beer law, $\bar{\kappa}$ can be calculated and expressed as:

$$\bar{\kappa} = -\frac{1}{L_m}\ln(1-\varepsilon) \tag{13}$$

where ε is the total emissivity of the gas calculated by WSGG model. L_m is the mean path length, which for any arbitrary shape can be expressed as:

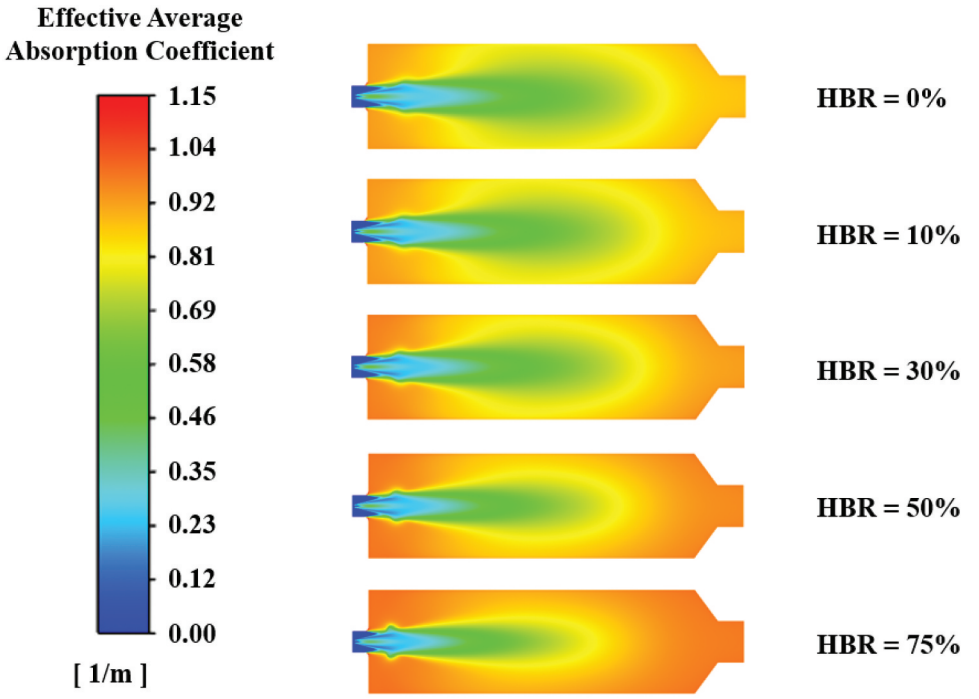

Figure 12. Distribution contour of gas effective average absorption coefficients for each hydrogen blending ratio case.

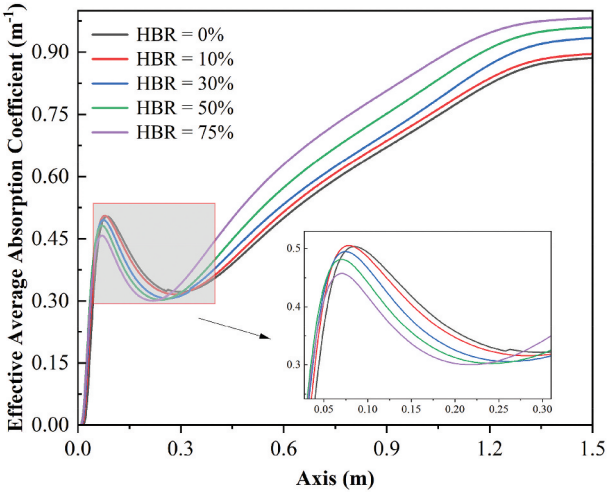

Figure 13. Axial distribution of gas effective average absorption coefficients for each hydrogen blending ratio case.

$$L_m = \frac{3.6V}{A} \tag{14}$$

where V and A, respectively, represent the internal volume and total surface area of the furnace chamber.

As shown in Figure 12 and Figure 13, beyond $x > 0.3$ m, the effective average absorption coefficient $\bar{\kappa}$ progressively rises with the hydrogen blending ratio, following the same trend as the variation in the molar fractions of H_2O and CO_2 in the product gases, which proves that CO_2 and H_2O are the highly dominant elements in the absorption-emission medium. The region where $x < 0.3$ m is the main reaction zone of combustion, featuring two inflection points: when $x < 0.1$ m, due to hydrogen's lower activation energy compared to methane, its reaction with O_2 is more likely to occur, then a large amount of H_2O is generated at the front part of the flame combustion reaction, causing the effective average absorption coefficient to rise rapidly; when $x > 0.1$ m, the reaction of CH_4 produces a large amount of CO_2, leading to a reduction in the molar ratio of H_2O and CO_2. Based on the gas radiation characteristic calculations model (Jin et al. 2024), a higher molar ratio corresponds to a larger gas effective average absorption coefficient, and a lower ratio corresponds to a smaller one, which is consistent with the numerical simulation results. When $x > 0.3$ m, the decrease in gas temperature causes the effective average absorption coefficient to increase. In summary, the hydrogen blending ratio has a significant impact on the gas effective average absorption coefficient during the combustion process. By adjusting the

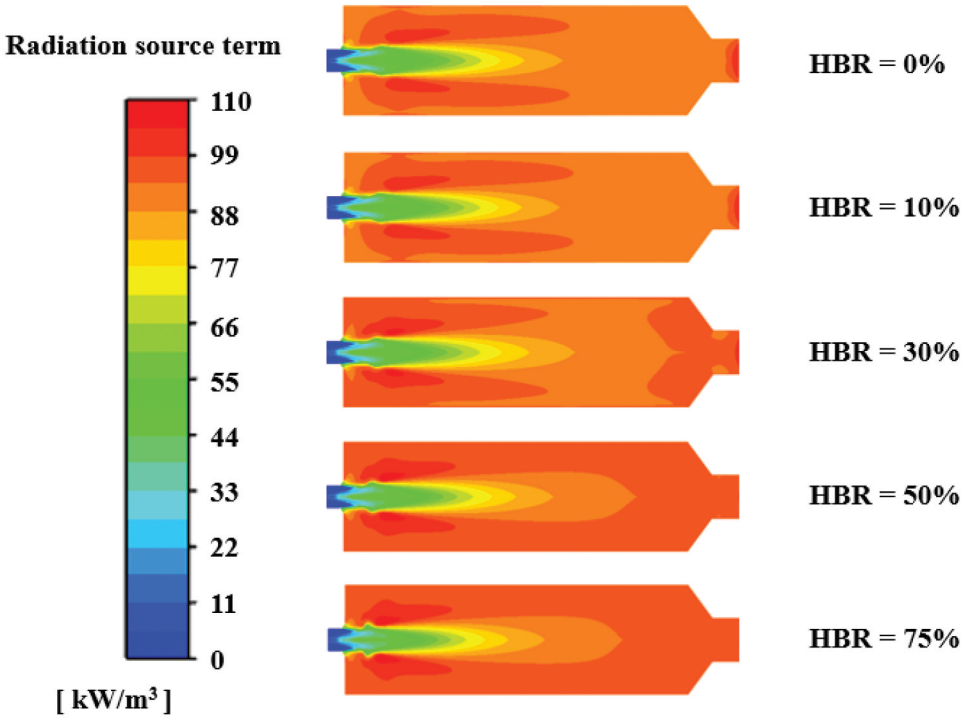

Figure 14. Distribution contour of the radiative source terms for each hydrogen blending ratio case.

hydrogen blending ratio, the composition of the product gases can be effectively altered, subsequently affecting their radiation characteristics.

The radiative heat source term, as a source term in the energy equation, plays a crucial role in the combustion process, directly influencing the temperature distribution and heat transfer process within the combustion chamber. Figure 14 clearly illustrates the distribution of the radiative source term within the combustion chamber, which is strongly related to the radiative energy density and serves as a key indicator for evaluating radiative heat transfer in furnace. In the primary reaction zone of combustion ($x < 0.3$ m), as the volume fractions of H_2O and CO_2 and the flame temperature increase, the radiative source term shows a gradually increasing trend, indicating that in the region where the combustion reaction is most intense, the radiative heat transfer intensity is also continuously increasing. At the same time, the peak of the radiative source term occurs at the location where the temperature and flue gas volume fraction reach their maximum values. This result further confirms the close correlation between the radiative heat source term and the temperature, product gas concentration within the combustion chamber. In regions with higher temperature and gas concentration, the intensity of radiative heat transfer also increases accordingly. The radiative heat source term plays a notable role in the combustion process, evolving with the advancement of the combustion reaction and changes in flame temperature and gas mixture composition.

To attain a deeper understanding of the radiative heat transfer characteristics in the front, middle, and rear stages of the combustion reaction, the radial distributions of temperature and absorption coefficient at three key positions are analyzed: $x = 0.05$ m, $x = 0.15$ m, and $x = 0.3$ m. As shown in Figure 15, in the front and middle stages of the combustion reaction, the flame temperature is lower near the central axis, while the effective average absorption coefficient is higher. Moreover, with an increase in the hydrogen

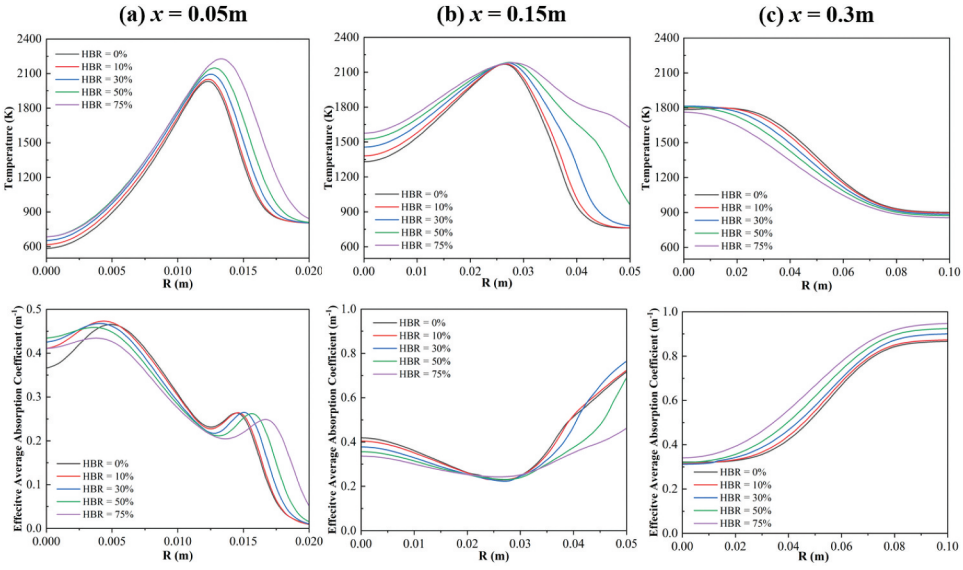

Figure 15. Radial distribution of temperatures and effective average absorption coefficients in the front, middle, and rear parts of the flame.

blending ratio, the flame temperature rises. At the front stage $x = 0.05$ m, as the radial distance increases, the flame and flue gas temperatures gradually rise, while the effective average absorption coefficient shows a decreasing trend. At the same time, the radiative source term also decreases, indicating that in the front stage of the combustion reaction, the gas radiation weakens as it moves away from the central axis of the flame. With further increase in radial distance, the gas temperature reaches a peak and then decreases. At this time, the effective average absorption coefficient initially rises briefly due to the temperature decline and then decreases as the molar fraction of the radiative gases reduces. In the middle and rear stages ($x = 0.15$ m and $x = 0.3$ m) of the reaction, the molar fraction of the gases stabilizes, and the gas effective average absorption coefficient mainly varies with temperature, showing an inverse relationship. Through the analysis of the radial distributions of temperature and effective average absorption coefficient at key positions, initial insights into the radiative heat transfer characteristics at various positions and stages of the combustion reaction are obtained. These results provide important theoretical foundations for further optimizing the combustion process and improving energy utilization efficiency.

Effect of hydrogen blending ratio on radiative heat transfer in combustion furnace

From the comparison of the above research results, it is evident that radiation can not be easily neglected in hydrogen-blended natural gas combustion simulations, as it influences the distributions of the temperature and component field inside the furnace. The most important parameter describing the overall radiation field of the flame is the net radiative heat transfer power Q_{net}, and its normalized variable, the "radiation fraction" f_{rad}, defined as the ratio of the radiative heat transfer power to the heat input from the fuel (Li and Modest 2003; Yang et al. 2018):

$$f_{rad} = \frac{Q_{net}}{m_{fuel}\Delta H_{comb}} \tag{15}$$

where m_{fuel} is the mass flow rate of the fuel, ΔH_{comb} is the specific heat of the mixed fuel. The net radiative heat transfer power Q_{net} is obtained by multiplying the radiative heat flux on the inner wall of the furnace by the area. The working conditions designed are shown in Table 4.

Figure 16 shows that under the condition of a constant fuel volumetric flow rate, the total heat input from the fuel gradually decreases with the hydrogen proportion, and the radiative heat transfer power also presents a downward trend. However, as the volumetric proportion of hydrogen increases, the radiation fraction rises. This indicates that with the

Table 4. Fuel input conditions and radiative heat transfer comparison.

HBR	Q_{net}(kW)	m_{fuel}(g/s)	ΔH_{comb}(kJ/kg)
0	12.169	0.86	51980.7
10	11.437	0.78	52979.6
20	10.681	0.71	54190.4
30	9.916	0.63	55688.5
40	9.155	0.56	57590.0
50	8.353	0.48	60083.0
70	6.692	0.33	68446.7
75	6.260	0.30	71868.2

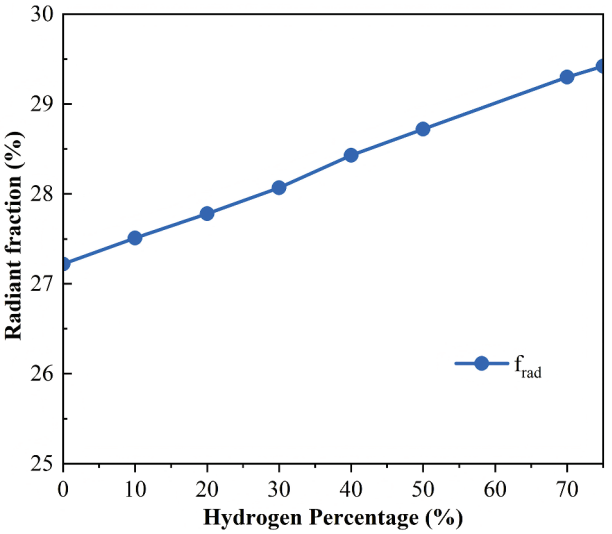

Figure 16. Results of radiation fraction variation for each hydrogen blending ratio case.

increase in the hydrogen blending ratio, the proportion of radiative heat transfer power in the combustion chamber also increases. Particularly for combustion with a hydrogen proportion of 75%, the radiation fraction reaches 29.42%, which represents a significant improvement compared to cases with no hydrogen blended or low hydrogen blending ratios. The increase in the radiation fraction ratio can be attributed to the characteristics of hydrogen combustion. The increased concentration of H_2O produced by hydrogen combustion, along with a notable rise in the H_2O/CO_2 molar ratio of the products, strengthens the radiation absorption of gas, resulting in higher radiative heat transfer power. The results demonstrate that the increase in the hydrogen blending ratio not only affects the heat input from the fuel but also significantly changes the proportion of radiative heat transfer power within the combustion chamber, which is of great significance for optimizing the combustion process, improving energy utilization efficiency, and reducing environmental pollution. By controlling the hydrogen blending ratio appropriately, the overall performance of the combustion system can be enhanced while maintaining combustion efficiency.

Conclusions

This study conducts numerical simulations of gas mixture combustion with different hydrogen proportions, quantitatively studied the temperature distribution, major combustion product concentration distribution, and radiation fraction changes in the combustion field under different hydrogen blending ratios. A new radiation characteristic WSGG model tailored for hydrogen blended natural gas combustion is applied to a hot co-flow combustor. The radiation characteristics of the flame and flue gas in a 40 kW combustion furnace are investigated, with a focus on the impact of different hydrogen blending ratios on fuel combustion temperature, gas effective average absorption coefficient, and radiative heat transfer. The main findings are as follows:

- Through comparison with published experimental data, the numerical simulation approach integrated with the new WSGG radiation model is verified to be able to provide reliable temperature gradients and gas mass fraction distributions. In particular, the simulated radial distribution of H_2O mass fraction at the position $x = 30$ mm of the flow field has an average error of only 7.7% with the experimental test point, which proves that the numerical simulation of the new WSGG model for calculating the natural gas hydrogen blended combustion conditions is quite reasonable, and the numerical simulation approach used is rational.
- As the hydrogen blending ratio increases, the temperature in combustion region increases and the position of the flame high-temperature region is advanced. Due to the decreasing total fuel heat load, the total heat released from the fuel combustion reduces, and the temperature at the combustion outlet becomes progressively lower. With the increase of hydrogen blending ratio from 0% to 75%, the peak temperature in the combustion region rises from 2180.5 K to 2291.8 K, while the outlet temperature decreases from 864 K to 815 K.
- In terms of the radiation characteristics of the flame flue gas, the effective average absorption coefficient of the overall gas grows gradually with the increase of hydrogen blending ratio from 0% to 75%, and at the axial $x = 0.6$ m point, the effective average absorption coefficient rises from 0.50 to 0.63, with an increase of more than 25%. This follows the same trend as the molar fraction ratio of H_2O to CO_2 in the reaction products, proving that H_2O and CO_2 are highly dominant factors in the absorption-emission medium. By adjusting the hydrogen blending ratio, the composition of the product gases can be effectively altered, subsequently affecting the radiation characteristics.
- In terms of the radiative heat transfer in the combustion chamber, for a constant fuel volume flow rate, the heat input of the fuel reduces with hydrogen blending ratio, and the radiative heat transfer decreases accordingly, while the radiation fraction ratio increases. Compared to pure natural gas combustion, the 75% hydrogen blended condition is able to increase the radiative fraction from 27.22% to 29.42%, indicating that the increase in hydrogen blending ratio enhances the proportion of radiative heat transfer to the total heat input.

From the above conclusions, the accurate radiation evaluation cannot be easily neglected in hydrogen-blended natural gas combustion simulation. It is advisable to use an accurate radiation characteristic simulation model, which is helpful to accurately obtain the characteristics of temperature, component, and radiative heat transfer. As the hydrogen blending ratio increases, the radiative fraction between the flue gases and global furnace walls increases, which provides a reference for optimizing hydrogen-blended combustion systems in natural gas boiler applications. However, due to the changes in combustion characteristics brought about by the high hydrogen blending ratio, the problems of combustion instability and NOx emission control still require further research.

Disclosure statement

No potential conflict of interest was reported by the author(s).

Funding

This work was supported by National Key Research and Development Program of China [2022YFB4003902], National Natural Science Foundation of China [52206175], Scientific Research Fund of Zhejiang Provincial Education Department [Y202457107] and Fundamental Research Funds for the Central Universities [2022ZFJH004].

References

Ballester, J., R. Hernández, A. Sanz, A. Smolarz, J. Barroso, and A. Pina. 2009. Chemiluminescence monitoring in premixed flames of natural gas and its blends with hydrogen. *Proc. Combust. Inst.* 32 (2):2983–91. doi: 10.1016/j.proci.2008.07.029.

Breer, B., H. Rajagopalan, C. Godbold, H. Johnson, B. Emerson, V. Acharya, W. Sun, D. Noble, and T. Lieuwen. 2023. Numerical investigation of NO_X production from premixed hydrogen/methane fuel blends. *Combust Flame* 255:112920. doi: 10.1016/j.combustflame.2023.112920.

Büyükakın, M. K., and S. Öztuna. 2020. Numerical investigation on hydrogen-enriched methane combustion in a domestic back-pressure boiler and non-premixed burner system from flame structure and pollutants aspect. *Int. J. Hydrogen Energy* 45 (60):35246–56. doi: 10.1016/j.ijhydene.2020.03.117.

Chen, Y., J. Niu, W. Liu, L. Long, T. Huang, Y. Sun, Z. Wan, and B. Yu. 2024. Experimental analysis and modeling on the blending limit of domestic burner with porous media for hydrogen enriched natural gas. *Int. J. Hydrogen Energy* 88:1321–31. doi: 10.1016/j.ijhydene.2024.09.263.

Choudhuri, A. R., and S. R. Gollahalli. 2004. Intermediate radical concentrations in hydrogen–natural gas blended fuel jet flames. *Int. J. Hydrogen Energy* 29 (12):1293–302. doi: 10.1016/j.ijhydene.2003.12.006.

Christo, F. C., G. G. Szego, and B. B. Dally. 2005. Modelling turbulent reacting jets under MILD combustion conditions. *5th Asia-Pacific Conference on Combustion, ASPACC 2005: Celebrating Prof. Bob Bilger's 70th Birthday*, Adelaide, South Australia, 329–32.

da Fonseca, R. J. C., G. C. Fraga, F. R. Coelho, and F. H. R. França. 2023. A wide-band based weighted-sum-of-gray-gases model for participating media: Application to H_2O-CO_2 mixtures with or without soot. *Int. J. Heat Mass Transf.* 204:123839. doi:10.1016/j.ijheatmasstransfer.2022.123839.

Dally, B. B., A. N. Karpetis, and R. S. Barlow. 2002. Structure of turbulent non-premixed jet flames in a diluted hot co-flow. *Proc. Combust. Inst.* 29 (1):1147–54. doi: 10.1016/S1540-7489(02)80145-6.

El-Ghafour, S. A. A., A. H. E. El-Dein, and A. A. R. Aref. 2010. Combustion characteristics of natural gas–hydrogen hybrid fuel turbulent diffusion flame. *Int. J. Hydrogen Energy* 35 (6):2556–65. doi: 10.1016/j.ijhydene.2009.12.049.

Fan, B., Y. Zhang, J. Pan, Y. Liu, W. Chen, P. Otchere, A. Wei, and R. He. 2018. The influence of hydrogen injection strategy on mixture formation and combustion process in a port injection (PI) rotary engine fueled with natural gas/hydrogen blends. *Energy Convers. Manag.* 173:527–38. doi: 10.1016/j.enconman.2018.08.002.

Gheshlaghi, M. K. G., and A. M. Tahsini. 2023. Numerical investigation of hydrogen addition effects to a methane-fueled high-pressure combustion chamber. *Int. J. Hydrogen Energy* 48 (86):33732–45. doi: 10.1016/j.ijhydene.2023.05.119.

Hottel, H. C., and A. F. Sarofim. 1967. *Radiative transfer*. (NY): Wiley.

Hou, F., Y. Liu, Z. Ma, C. Liu, S. Zhang, F. Yang, and Y. Nie. 2023. Study of the carbon neutral path in China: A literature review. *Chn. J. Urb. Environ. Stud.* 11 (2):2350008. doi: 10.1142/S2345748123500082.

Jiang, X., P. Li, J. Guo, F. Hu, F. Wang, J. Mi, and Z. Liu. 2018. Detailed investigation of NO mechanism in non-premixed oxy-fuel jet flames with CH_4/H_2 fuel blends. *Int. J. Hydrogen Energy* 43 (17):8534–57. doi: 10.1016/j.ijhydene.2018.03.100.

Jin, G., S. Shan, X. Wang, J. Yu, Z. Wang, and Z. Zhou. 2024. New multi-parametrical pressurized WSGG model correlations for gaseous radiative heat transfer in high H_2O/CO_2 molar ratio

conditions for sustainable fuel utilization. *Int. J. Hydrogen Energy* 69:173–83. doi: 10.1016/j.ijhydene.2024.04.367.

Ju, Y., G. Masuya, and P. D. Ronny. 1998. Effects of radiative emission and absorption on the propagation and extinction of premixed gas flames. *Symp. Int. Combust.* 27 (2):2619–26. doi: 10.1016/S0082-0784(98)80116-1.

Kuo, K. K. 1986. *Principles of combustion*. (NY): Wiley.

Li, G., and M. F. Modest. 2003. Importance of turbulence-radiation interactions in turbulent diffusion Jet flames. *ASME. J. Heat. Mass. Transf.* 125 (5):831–38. doi:10.1115/1.1597621.

Patel, V., and R. Shah. 2019. Effect of hydrogen enrichment on combustion characteristics of methane swirling and non-swirling inverse diffusion flame. *Int. J. Hydrogen Energy* 44 (52):28316–29. doi: 10.1016/j.ijhydene.2019.09.076.

Poinsot, T., and D. Veynante. 2005. *Theoretical and numerical combustion*. Philadelphia: R. T. Edwards.

Rajpara, P., R. Shah, and J. Banerjee. 2018. Effect of hydrogen addition on combustion and emission characteristics of methane fuelled upward swirl can combustor. *Int. J. Hydrogen Energy* 43 (36):17505–19. doi: 10.1016/j.ijhydene.2018.07.111.

Ren, H. S., J. B. Wang, and X. Y. Li. 2021. Combustion dynamics, Sichuan. Accessed December 1, 2024. http://cds.scu.edu.cn/ .

Shan, S., B. Qian, Z. Zhou, Z. Wang, and K. Cen. 2018. New pressurized WSGG model and the effect of pressure on the radiation heat transfer of H_2O/CO_2 gas mixtures. *Int. J. Heat Mass Transf.* 121:999–1010. doi:10.1016/j.ijheatmasstransfer.2018.01.079.

Smith, T. F., Z. F. Shen, and J. N. Friedman. 1982. Evaluation of coefficients for the weighted sum of gray gases model. *J. Heat Transf.* 104 (4):602–08. doi:10.1115/1.3245174.

Wang, C. J., J. X. Wen, Z. B. Chen, and S. Dembele. 2014. Predicting radiative characteristics of hydrogen and hydrogen/methane jet fires using FireFOAM. *Int. J. Hydrogen Energy* 39 (35):20560–69. doi: 10.1016/j.ijhydene.2014.04.062.

Wang, G., X. Liu, P. Li, G. Shi, X. Cai, Z. Liu, and J. Mi. 2024. MILD combustion of a premixed NH_3 /air jet flame in hot coflow versus its CH_4/air counterpart. *Fuel* 355:129523. doi:10.1016/j.fuel.2023.129523.

Xu, S., Z. Tian, Y. Chen, S. Liang, Y. Tu, and H. Liu. 2024. Effect of hydrogen-blending ratio and wall temperature on establishment, NO formation, and heat transfer of hydrogen-enriched methane MILD combustion. *Fuel* 369:131787. doi:10.1016/j.fuel.2024.131787.

Yang, X., Z. He, S. Dong, and H. Tan. 2018. Prediction of turbulence radiation interactions of CH_4-H_2 /air turbulent flames at atmospheric and elevated pressures. *Int. J. Hydrogen Energy* 43 (32):15537–50. doi: 10.1016/j.ijhydene.2018.06.060.

Yin, C., L. C. R. Johansen, L. A. Rosendahl, and S. K. Kær. 2010. New weighted sum of gray gases model applicable to computational fluid dynamics (CFD) modeling of oxy–fuel combustion: Derivation, validation, and implementation. *Energy Fuels* 24 (12):6275–82. doi: 10.1021/ef101211p.

Yoon, J., S. Joo, J. Kim, M. C. Lee, J. G. Lee, and Y. Yoon. 2017. Effects of convection time on the high harmonic combustion instability in a partially premixed combustor. *Proc. Combust. Inst.* 36 (3):3753–61. doi:10.1016/j.proci.2016.06.105.

Zareei, J., A. Rohani, and W. M. F. W. Mahmood. 2018. Simulation of a hydrogen/natural gas engine and modelling of engine operating parameters. *Int. J. Hydrogen Energy* 43 (25):11639–51. doi: 10.1016/j.ijhydene.2018.02.047.

Zenou, J. B., and R. Vicquelin. 2025. Coupling regimes of premixed laminar flames with thermal radiation absorption in fresh gases. Application to H_2O-/CO_2-diluted mixtures. *Combust. Flame* 271:113830. doi:10.1016/j.combustflame.2024.113830.

Zhao, K., D. Cui, T. Xu, Q. Zhou, S. Hui, and H. Hu. 2008. Effects of hydrogen addition on methane combustion. *Fuel Process Technol.* 89 (11):1142–47. doi:10.1016/j.fuproc.2008.05.005.

Zheng, S., H. Liu, D. Li, Z. Liu, B. Zhou, and Q. Lu. 2022. Effects of radiation reabsorption on the laminar burning velocity of methane/air and methane/hydrogen/air flames at elevated pressures. *Fuel* 311:122586. doi:10.1016/j.fuel.2021.122586.

Zohera, K. F., A. Mounir, and C. Salah. 2017. Numerical simulation of CH_4-H_2-AIR non-premixed flame stabilized by a bluff body. *Energy Procedia* 139:530–36. doi: 10.1016/j.egypro.2017.11.249.